

# PAPR Reduction with Pre-chirp Selection for Affine Frequency Division Multiplexing

Haozhi Yuan<sup>1</sup>, Yin Xu<sup>1</sup>, *Senior Member, IEEE*, Xinghao Guo<sup>1</sup>, Yao Ge<sup>2</sup>, *Member, IEEE*, Tianyao Ma<sup>1</sup>,  
Haoyang Li<sup>1</sup>, *Member, IEEE*, Dazhi He<sup>1</sup>, *Senior Member, IEEE*, Wenjun Zhang<sup>1</sup>, *Fellow, IEEE*

**Abstract**—Affine frequency division multiplexing (AFDM) is a promising new multicarrier technique for high-mobility communications based on discrete affine Fourier transform (DAFT). By properly tuning the pre-chirp parameter and the post-chirp parameter in the DAFT, the effective channel in the DAFT domain can completely circumvent path overlap, thereby constituting a full representation of delay-Doppler profile. However, AFDM has a crucial problem of high peak-to-average power ratio (PAPR), stemming from randomness of modulated symbols. In this letter, a novel algorithm named grouped pre-chirp selection (GPS) is proposed to reduce PAPR by strategically varying the pre-chirp parameter across subcarrier groups. Initially, it is established that key AFDM properties are maintained when implementing GPS. Next, we proceed to detail the operational procedures of the GPS algorithm, elucidating its principle for PAPR reduction and emphasizing its computational efficiency advantages. Finally, simulation results employing the complementary cumulative distribution function (CCDF) validate the effectiveness of the proposed GPS in reducing PAPR.

**Index Terms**—Affine frequency division multiplexing (AFDM), discrete affine Fourier transform (DAFT), grouped pre-chirp selection (GPS), peak-to-average power ratio (PAPR), complementary cumulative distribution function (CCDF).

## I. INTRODUCTION

THE next generation wireless systems (beyond 5G/6G) is anticipated to accommodate high-mobility scenarios such as vehicle-to-everything (V2X) systems, high-speed railway systems, and unmanned aerial vehicle (UAV) communications [1]. The high velocities between transmitters and receivers can lead to substantial Doppler frequency shifts which cause the wireless channel to exhibit fast time-varying characteristics. In existing 4G/5G standards, the prevalent multicarrier technique, i.e., orthogonal frequency division multiplexing (OFDM), exhibits limited robustness against carrier frequency offset (CFO) [2]. Consequently, the system performance of OFDM degrades significantly in high-mobility scenarios.

In this context, a series of advanced waveform designs are proposed. Among these, affine frequency division multiplexing

(AFDM) stands out as a promising multicarrier modulation scheme utilizing the discrete affine Fourier transform (DAFT) [3], [4]. By appropriately tuning two DAFT chirp parameters, here called the pre-chirp parameter and the post-chirp parameter, subchannels originating from different propagation paths can be completely separated. This process leads to a sparse and quasi-static representation of the effective channel in the DAFT domain, thereby enabling AFDM to attain full diversity order in doubly dispersive channels. Moreover, DAFT serves as a generalized form of the discrete Fourier transform (DFT), ensuring AFDM to remain fully compatible with OFDM. Compared to orthogonal time frequency space (OTFS) [5], another emerging multicarrier technique for high-mobility communications, AFDM requires less pilot guard overhead and has lower modulation complexity [6]. AFDM has garnered increasing attention in the literature due to its advantages in high-mobility communications and compatibility. Recent studies have focused on various aspects of AFDM system such as channel estimation [7], equalization [8], index modulation (IM) [9], non-orthogonal multiple access (NOMA) [10], and integrated sensing and communication (ISAC) methods [11].

Despite the advantages, AFDM encounters a critical challenge of high peak-to-average power ratio (PAPR), which is theoretically identical to that in OFDM. High PAPR levels lead to power amplifier saturation at the transmitter, ultimately deteriorating communication reliability. In OFDM, there are several methods for PAPR reduction, such as coding [12], selective mapping (SLM) [13], Tone Reservation (TR) [14], and other schemes. However, to the best of our knowledge, no studies currently exist on PAPR reduction for AFDM.

In this letter, a grouped pre-chirp selection (GPS) algorithm is proposed to reduce PAPR in AFDM. Given the loose constraint on the pre-chirp parameter, there exists an opportunity to reduce PAPR by substituting the original uniform pre-chirp parameter across all subcarriers with a distinct pre-chirp parameter on each subcarrier. While theoretically, enumerating all feasible pre-chirp parameter values across every subcarrier could minimize PAPR, such an exhaustive approach entails significant computational costs. Instead, a non-enumerated algorithm is employed to mitigate computational complexity, while subcarriers are grouped based on specific criteria.

## II. SYSTEM MODEL

### A. Conventional AFDM

The conventional AFDM block diagram is depicted in Fig. 1. Data symbols are initially placed in the DAFT domain. At

This paper is supported in part by National Natural Science Foundation of China Program (62271316, 62371291, 62101322), National Key R&D Project of China (2023YFF0904603), the Fundamental Research Funds for the Central Universities and Shanghai Key Laboratory of Digital Media Processing (STCSM 18DZ2270700). (*Corresponding author: Yin Xu.*)

Haozhi Yuan, Yin Xu, Xinghao Guo, Tianyao Ma, Haoyang Li, Dazhi He, and Wenjun Zhang are with the Cooperative Medianet Innovation Center, Shanghai Jiao Tong University, Shanghai 200240, China (e-mail: xuyin@sjtu.edu.cn).

Yao Ge is with the Continental-NTU Corporate Lab, Nanyang Technological University, Singapore 639798.

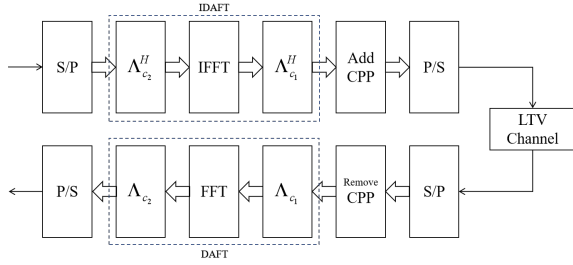


Fig. 1. AFDM block diagram.

the transmitter, inverse DAFT (IDAFT) is employed to map the symbols from the DAFT domain into the time domain. With  $N$  chirp subcarriers, the IDAFT operation can be formulated as

$$s[n] = \frac{1}{\sqrt{N}} \sum_{m=0}^{N-1} x[m] \cdot e^{j2\pi(c_1 n^2 + c_2 m^2 + mn/N)}, \quad (1)$$

where  $x[m]$  denotes the modulated symbol in the DAFT domain, and  $s[n]$  signifies the signal in the time domain. According to (1), the frequencies of all subcarriers exhibit periodic and linear variations over time in AFDM. After adding chirp-periodic prefix (CPP), the time-domain signal  $s[n]$  undergoes propagation through the linear time-varying (LTV) channel whose impulse response can be represented as

$$h_n[l] = \sum_{p=1}^P h_p e^{-j2\pi f_p n} \delta(l - l_p), \quad (2)$$

where  $P$  is the number of paths,  $\delta(\cdot)$  is the Dirac delta function,  $h_p$ ,  $f_p$ , and  $l_p$  are the complex gain, Doppler shift, and the integer delay associated with the  $p$ -th path, respectively.

For data symbols within each block, the DAFT/IDAFT operations and the effect of the LTV channel can both be expressed in matrix form. The input-output relation in the time domain, i.e., the effect of the LTV channel at the receiver, can be formulated as

$$\mathbf{r} = \mathbf{H}\mathbf{s} + \mathbf{w}, \quad (3)$$

where  $\mathbf{s}$ ,  $\mathbf{r} \in \mathbb{C}^{N \times 1}$ ,  $\mathbf{w} \sim \mathcal{CN}(\mathbf{0}, N_0 \mathbf{I}) \in \mathbb{C}^{N \times 1}$ , and

$$\mathbf{H} = \sum_{p=1}^P h_p \mathbf{\Gamma}_{\text{CPP}_p} \mathbf{W}^{f_p} \mathbf{\Pi}^{l_p}, \quad (4)$$

where  $\mathbf{\Pi}$  is the permutation matrix

$$\mathbf{\Pi} = \begin{bmatrix} 0 & \cdots & 0 & 1 \\ 1 & \cdots & 0 & 0 \\ \vdots & \ddots & \ddots & \vdots \\ 0 & \cdots & 1 & 0 \end{bmatrix}_{N \times N}, \quad (5)$$

$\mathbf{W}$  is the diagonal matrix

$$\mathbf{W} = \text{diag}(e^{-j2\pi n}, n = 0, 1, \dots, N-1), \quad (6)$$

and  $\mathbf{\Gamma}_{\text{CPP}_p}$  is an  $N \times N$  diagonal matrix

$$\mathbf{\Gamma}_{\text{CPP}_p} = \text{diag} \left( \begin{cases} e^{-j2\pi c_1 (N^2 - 2N(l_p - n))} & n < l_p, n = 0, \dots, N-1 \\ 1 & n \geq l_p \end{cases} \right). \quad (7)$$

The DAFT matrix is expressed as

$$\mathbf{A} = \mathbf{\Lambda}_{c_2} \mathbf{F} \mathbf{\Lambda}_{c_1}, \quad (8)$$

where  $\mathbf{F} \in \mathbb{C}^{N \times N}$  is the normalized  $N$ -point DFT matrix and

$$\mathbf{\Lambda}_{c_i} = \text{diag}(e^{-j2\pi c_i n^2}, n = 0, 1, \dots, N-1, i = 1, 2). \quad (9)$$

It is obvious that  $\mathbf{A}$  is unitary. Consequently, the IDAFT matrix can be expressed as

$$\mathbf{A}^{-1} = \mathbf{A}^H = \mathbf{\Lambda}_{c_1}^H \mathbf{F}^H \mathbf{\Lambda}_{c_2}^H. \quad (10)$$

Let  $\mathbf{x} = [x[0], x[1], \dots, x[N-1]]^T \in \mathbb{C}^{N \times 1}$  denotes the symbols in the DAFT domain at the transmitter, where each element resides at a constellation point. Similarly, let  $\mathbf{y} = [y[0], y[1], \dots, y[N-1]]^T \in \mathbb{C}^{N \times 1}$  denotes the received signal in the DAFT domain. The comprehensive input-output relation in the DAFT domain can thus be formulated as

$$\mathbf{y} = \mathbf{A}\mathbf{r} = \sum_{p=1}^P h_p \mathbf{A} \mathbf{\Gamma}_{\text{CPP}_p} \mathbf{W}^{f_p} \mathbf{\Pi}^{l_p} \mathbf{A}^H \mathbf{x} + \mathbf{A}\mathbf{w} = \mathbf{H}_{\text{eff}} \mathbf{x} + \tilde{\mathbf{w}}, \quad (11)$$

where  $\tilde{\mathbf{w}} \sim \mathcal{CN}(\mathbf{0}, N_0 \mathbf{I}) \in \mathbb{C}^{N \times 1}$  still holds due to  $\mathbf{A}$  being a unitary matrix, and

$$\mathbf{H}_{\text{eff}} = \sum_{p=1}^P h_p \mathbf{A} \mathbf{\Gamma}_{\text{CPP}_p} \mathbf{W}^{f_p} \mathbf{\Pi}^{l_p} \mathbf{A}^H. \quad (12)$$

According to [3], achieving full diversity in LTV channels with integer Doppler shift requires setting the pre-chirp parameter  $c_2$  to any irrational value. Additionally, the minimum permissible value for the post-chirp parameter  $c_1$  is given by

$$c_1 = \frac{2\alpha_{\max} + 1}{2N}, \quad (13)$$

where  $\alpha_{\max}$  is the integer part of the maximum Doppler shift normalized with respect to the subcarrier spacing. The value of  $c_1$  is crucial for AFDM to achieve full diversity, whereas the constraint on  $c_2$  is loose, which provides sufficient flexibility to reduce PAPR by optimizing  $c_2$ .

## B. AFDM with GPS

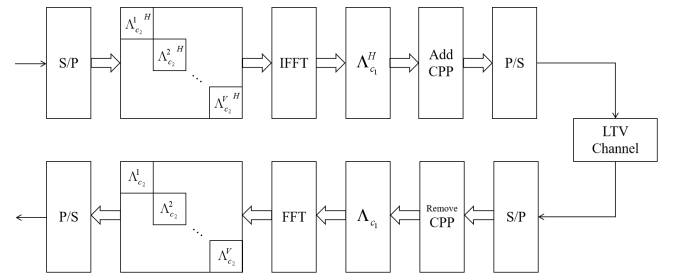


Fig. 2. AFDM with GPS block diagram.

The block diagram depicted in Fig. 2 illustrates AFDM with GPS, where the pre-chirp module is the only module that differs from the conventional AFDM shown in Fig. 1. The pre-chirp module are divided into  $V$  groups, each containing

$M = \frac{N}{V}$  pre-chirp subcarriers. Consequently, the subdiagonal matrix of each group can be expressed as

$$\Lambda_{c_2}^v = \text{diag}(e^{-j2\pi c_{2,m} m^2}, m = (v-1)M, \dots, vM-1), \quad (14)$$

where  $v = 1, \dots, V$ . Distinct  $c_2$  values are employed across each subcarrier, where  $c_{2,m} \in \Omega_m$  denotes the value of  $c_2$  on the  $m$ -th subcarrier, and  $\Omega_m$  represents the set of feasible values for  $c_2$ . It should be emphasized that within the  $v$ -th group, all  $c_{2,m}$  share a common element index  $i_v$  in  $\Omega_m$ , rather than the same specific value. The resultant time-domain signals can be mathematically represented as

$$s[n] = \frac{1}{\sqrt{N}} \sum_{m=0}^{N-1} x[m] \cdot e^{j2\pi(c_1 n^2 + c_{2,m} m^2 + mn/N)}. \quad (15)$$

Such a modification is intended to reduce the PAPR. However, it is crucial to assess whether the original properties of AFDM still hold, which will be elaborated upon subsequently.

Primarily, the orthogonality between any pair of subcarriers remains unaffected. This assertion can be deduced as follows: considering two subcarriers with identical  $c_1$  but differing  $c_2$ , expressed as  $e^{j2\pi(c_1 n^2 + c_{2,m_1} m_1^2 + m_1 n/N)}$  and  $e^{j2\pi(c_1 n^2 + c_{2,m_2} m_2^2 + m_2 n/N)}$ , where  $c_{2,m_1}$  and  $c_{2,m_2}$  are distinct irrational numbers satisfying  $c_{2,m_1} \neq c_{2,m_2}$ . Their inner product can be derived as

$$\begin{aligned} & \sum_{n=0}^{N-1} e^{j2\pi(c_1 n^2 + c_{2,m_1} m_1^2 + m_1 n/N)} e^{-j2\pi(c_1 n^2 + c_{2,m_2} m_2^2 + m_2 n/N)} \\ &= e^{j2\pi(c_{2,m_1} m_1^2 - c_{2,m_2} m_2^2)} \sum_{n=0}^{N-1} e^{j\frac{2\pi}{N}(m_1 - m_2)n} \\ &= e^{j2\pi(c_{2,m_1} m_1^2 - c_{2,m_2} m_2^2)} \frac{1 - e^{j2\pi N(\frac{m_1 - m_2}{N})}}{1 - e^{j2\pi(\frac{m_1 - m_2}{N})}} \\ &= 0 \quad (0 \leq m_1 < m_2 \leq N-1). \end{aligned} \quad (16)$$

The derivation above establishes that such a modification does not affect the orthogonality.

Furthermore, it is evident that the sparse property of the effective channel  $\mathbf{H}_{\text{eff}}$  persists. Given that both  $\Lambda_{c_2}^H$  and  $\Lambda_{c_2}$  are diagonal matrices, altering the values of the diagonal elements does not influence the locations of the non-zero elements. The persistence of the above properties forms the basis for our proposed GPS algorithm.

### III. PROPOSED PAPR REDUCTION SCHEME

In this section, the proposed GPS algorithm for PAPR reduction is elaborated. Within each block, the expression of PAPR is formulated as

$$\text{PAPR} = \frac{P_{\text{max}}}{P_{\text{avg}}} = \frac{\max_{n=0, \dots, N-1} (\|s[n]\|^2)}{\frac{1}{N} \sum_{n=0}^{N-1} \|s[n]\|^2}, \quad (17)$$

where  $s[n]$  is the  $n$ -th sample of the time-domain signals. Although PAPR is defined for continuous-time bandpass signals, with no less than 4-fold oversampling,  $s[n]$  and the continuous-time bandpass signals have almost the same PAPR [15]. To quantitatively characterize the PAPR metric, the

complementary cumulative distribution function (CCDF) is utilized, which is defined as

$$\text{CCDF} = \Pr(\text{PAPR} > \text{PAPR}_0), \quad (18)$$

where  $\text{PAPR}_0$  represents a specific threshold value of the PAPR, and  $\Pr(\cdot)$  denotes the probability function.

Based on the persistence of the original AFDM properties, the GPS tunes the values of  $c_2$  on each subcarrier by group in a non-enumerated manner and then selects the signal with the smallest PAPR among all the candidate signals. Compared to the optimal algorithm, the GPS greatly reduces the computational complexity with no significant performance degradation. The optimal algorithm is described as follows. Initially, finite sets  $\Omega_m$  ( $m = 1, \dots, N-1$ ) are created with irrational elements. Each  $\Omega_m$  is assumed to contain  $W$  elements. By exhaustively enumerating all possible values across every subcarrier, the optimal PAPR can theoretically be achieved. However, this approach incurs prohibitively high computational costs because each PAPR calculation involves an IFFT matrix multiplication and a subsequent post-chirp matrix multiplication, whose complexity is normalized to  $\mathcal{O}(1)$ . Consequently, a total of  $\mathcal{O}(W^{N-1})$  computational complexity are required to obtain the final result. Note that the first subcarrier (where  $m = 0$ ) requires no alteration as the initial phase remains constant at 0 according to (15), which corresponds to the exponent  $N-1$ . Given the impractically high computational complexity of the aforementioned method, achieving a balanced trade-off between performance and computational efficiency necessitates consideration of the following three aspects.

Initially, the principle governing the selection of elements in  $\Omega_m$  is considered. According to (15), the phase of each term in the summation process is given by  $\text{angle}(x[m]) + 2\pi(c_1 n^2 + c_{2,m} m^2 + mn/N)$ , where  $x[m]$  generates phase randomness. For a large number of subcarriers  $N$ , the phase randomness does not affect average power but significantly impacts peak power by causing notable fluctuations. Hence, minimizing peak power is paramount. For the sake of simplicity, we first consider the scenario where the set comprises two elements. The pre-chirp module rotates the phase of each data symbol. Since the algorithm picks out the smallest PAPR outcome, the phase difference of the two elements should be made as large as possible. This strategy derives from the constancy of expected peak power regardless of rotation; hence, a greater phase variance implies a smaller minimum peak power among all candidate signals. Following this principle, the optimal phase difference between elements is  $\pi$ , which can be formulated as

$$2\pi c_{2,m} m^2 = \pm \frac{\pi}{2}. \quad (19)$$

Then, the value of the pre-chirp parameter on the  $m$ -th subcarrier is given as

$$c_{2,m} = (-1)^i \frac{1}{4m^2}, \quad (20)$$

where  $i = 0, 1$  corresponds to the two elements in  $\Omega_m$ . However, given that the pre-chirp value should be irrational,

(20) is accordingly substituted with

$$c_{2,m} = (-1)^i \frac{\pi \cdot 10^k}{4m^2 \lfloor \pi \cdot 10^k \rfloor}, \quad (21)$$

where  $\lfloor \cdot \rfloor$  denotes the floor function, and  $k$  determines the precision of decimals retained. This principle can be generalized to cases where  $\Omega_m$  contains  $W$  ( $W \geq 2$ ) elements. The  $W$  feasible values of the pre-chirp parameter on the  $m$ -th subcarrier are

$$c_{2,m} = \frac{(i + \frac{1}{2})\pi \cdot 10^k}{Wm^2 \lfloor \pi \cdot 10^k \rfloor}, \quad (22)$$

where  $i = 0, \dots, W - 1$ . The increase in the number of elements in  $\Omega_m$  evidently promotes PAPR reduction. However, the phase difference between the elements inevitably diminishes as  $W$  increases. Consequently, the rate of performance enhancement gradually slows down while the complexity escalates linearly. Therefore, to achieve a good balance between performance and complexity, employing two or three elements in each  $\Omega_m$  may be sufficient, as substantiated by simulations.

Furthermore, adopting a non-enumerated algorithm with fewer iterations can substantially mitigate complexity. Specifically, the pre-chirp values in  $\Omega_m$  are sequentially selected across all subcarriers, rather than enumerating all possible permutations. Each pre-chirp adjustment that reduces PAPR will permanently replace the prior value; otherwise, it is reverted. Precisely, when  $W = 2$ , the computational complexity of the enumerated algorithm and the non-enumerated algorithm is  $\mathcal{O}(2^{N-1})$  and  $\mathcal{O}(N - 1)$ , respectively.

Moreover, complexity can be further alleviated by grouping subcarriers. The number of subcarriers included in any one group is arbitrary in principle, but each group is set to be of equal size for convenience. By dividing the subcarriers into  $V$  groups, the computational complexity is further reduced from  $\mathcal{O}(N - 1)$  to  $\mathcal{O}(V)$  per block. In addition to the number of groups, the grouping pattern also affects the performance. Two grouping patterns are considered: adjacent grouping (where adjacent subcarriers are grouped together) and comb grouping (where spaced subcarriers are grouped together). Simulation results indicate that adjacent grouping more effectively reduced PAPR compared to comb grouping, despite their equivalent computational complexity.

The proposed GPS with  $W = 2$  is outlined in Algorithm 1 as an example. The initialization step involves setting the pre-chirp value on each subcarrier to a positive number. Here, we set  $c_{2,m} = \frac{\pi}{12.56m^2}$  where  $k = 2$  on each subcarrier. Consequently, the initialized pre-chirp matrix is given as

$$\mathbf{\Lambda}_{c_2}^{(0)} = \text{diag} \left( 1, e^{j \frac{2\pi^2}{12.56}}, \dots, e^{j \frac{2\pi^2}{12.56}} \right)_{N \times N}. \quad (23)$$

The corresponding initial PAPR is subsequently computed as

$$\text{PAPR}^{(0)} = \frac{\max(|\mathbf{\Lambda}_{c_1}^H \mathbf{F}^H \mathbf{\Lambda}_{c_2}^{H(0)} \mathbf{x}|^2)}{\text{mean}(|\mathbf{\Lambda}_{c_1}^H \mathbf{F}^H \mathbf{\Lambda}_{c_2}^{H(0)} \mathbf{x}|^2)}. \quad (24)$$

During each iteration, the pre-chirp values within a designated group undergo complete reversal. Then, a new  $\text{PAPR}^{(l)}$  is calculated using an updated pre-chirp matrix  $\mathbf{\Lambda}_{c_2}^{(l)}$ . Upon completion of the algorithm, the minimum PAPR among  $(V + 1)$  values, denoted as  $\text{PAPR}_{\min}$ , along with its corresponding pre-chirp matrix  $\mathbf{\Lambda}_{c_2}^*$ , is selected as the output.

### Algorithm 1 GPS with $W = 2$ in AFDM System for PAPR Reduction

**Input:** Number of subcarriers  $N$ , number of groups  $V$ , number of subcarriers per group  $M$ , post-chirp matrix  $\mathbf{\Lambda}_{c_1}$ , normalized FFT matrix  $\mathbf{F}$ , symbol vector  $\mathbf{x}$ ;

- 1: Initialize  $\mathbf{\Lambda}_{c_2}^{(0)}$  and  $\text{PAPR}^{(0)}$  as (23) and (24), respectively;
- 2:  $\text{PAPR}_{\min} = \text{PAPR}^{(0)}$ ;
- 3: **for**  $l = 1 : V$  **do**
- 4:  $\mathbf{\Lambda}_{c_2}^{(l)} = \mathbf{\Lambda}_{c_2}^{(l-1)}$ ;
- 5:  $\mathbf{\Lambda}_{c_2}^{(l)}((l-1)M+1:LM) = \mathbf{\Lambda}_{c_2}^{(l-1)}((l-1)M+1:LM)^H$ ;
- 6: Calculate  $\text{PAPR}^{(l)}$  similar to (24);
- 7: **if**  $\text{PAPR}^{(l)} \geq \text{PAPR}_{\min}$  **then**
- 8:  $\mathbf{\Lambda}_{c_2}^{(l)}((l-1)M+1:LM) = \mathbf{\Lambda}_{c_2}^{(l-1)}((l-1)M+1:LM)^H$ ;
- 9: **else**
- 10:  $\text{PAPR}_{\min} = \text{PAPR}^{(l)}$ ;
- 11: **end if**
- 12: **end for**
- 13:  $\mathbf{\Lambda}_{c_2}^* = \mathbf{\Lambda}_{c_2}^{(V)}$ ;

**Output:**  $\text{PAPR}_{\min}$  and  $\mathbf{\Lambda}_{c_2}^*$ .

## IV. NUMERICAL RESULTS

An AFDM system with 16QAM under LTV channel is considered. Without loss of generality, channel coefficients  $h_i \sim \mathcal{CN}(0, 1)$  are generated. The number of subcarriers, elements per set, and groups are set as  $N = 64$ ,  $W = 2, 3, 4$ , and  $V = 4, 8, 16$ , respectively.

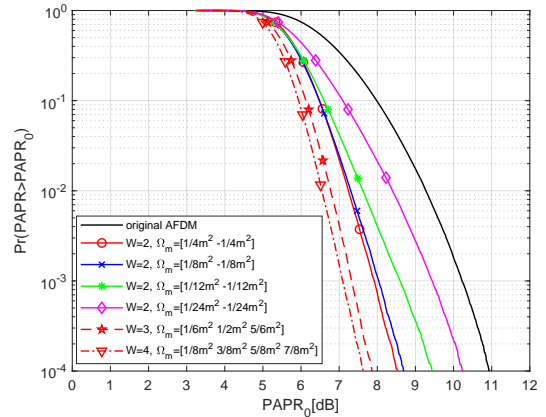


Fig. 3. PAPR performance of 16QAM AFDM system with GPS for different  $W$  and  $\Omega_m$ .

In Fig. 3, simulation results of GPS are presented for different values and number of elements in  $\Omega_m$ , where  $V = 4$  and adjacent grouping pattern are applied. In terms of values of elements, the results demonstrate that a larger phase difference yields improved performance, assuming an equivalent number of elements. In terms of number of elements  $W$ , the performance gain from the increase of number converges quickly. Compared with the original AFDM, a reduction in PAPR by approximately 2.5 dB can be achieved when  $W = 2$  and  $\Omega_m = [\frac{1}{4m^2}, -\frac{1}{4m^2}]$ .

Fig. 4 illustrates the impact of the number of groups and different grouping strategies on performance, where  $W = 2$

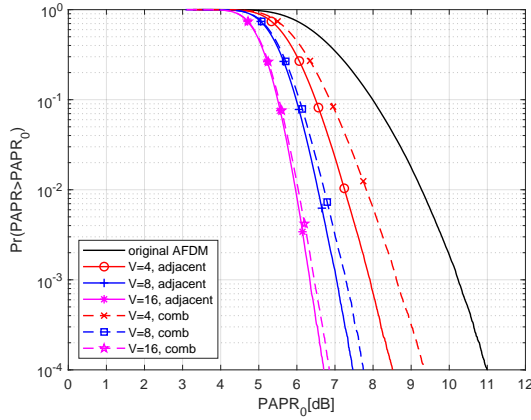


Fig. 4. PAPR performance of 16QAM AFDM system with GPS for different  $V$  and grouping patterns.

and  $\Omega_m = [\frac{1}{4m^2}, -\frac{1}{4m^2}]$  are employed. It can be observed that adjacent grouping consistently outperforms comb grouping. Targeting the CCDF at a level of  $10^{-4}$ , the adjacent grouping pattern demonstrates performance improvements of approximately 0.7 dB, 0.3 dB, and 0.1 dB over the comb grouping pattern for configurations with 4, 8, 16 groups, respectively. In addition, increasing the number of groups could enhance the effectiveness of PAPR reduction. However, the rate of performance improvement diminishes as the number of groups increases, which indicates a significant increase in complexity. To balance complexity and performance, it is advisable to keep the number of groups minimal, provided that the desired PAPR reduction threshold is achieved.

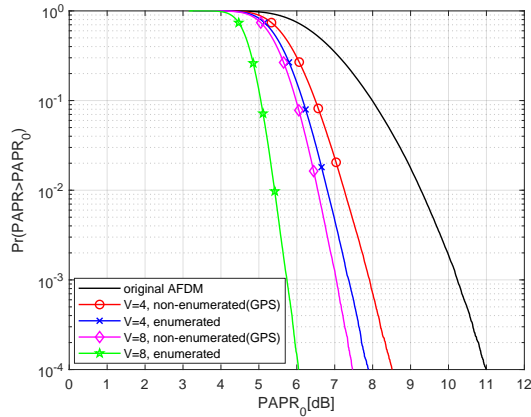


Fig. 5. PAPR performance of 16QAM AFDM system with GPS and enumerated algorithm.

In Fig. 5, the performance disparity between the enumerated algorithm and the GPS is depicted, where  $W = 2$ ,  $\Omega_m = [\frac{1}{4m^2}, -\frac{1}{4m^2}]$ , and the adjacent grouping pattern are applied. The enumerated algorithm consistently outperforms the non-enumerated algorithm. However, this enhancement comes at the cost of significantly increased computational complexity. Specifically, the computational complexity is  $\frac{2^V}{V}$  times higher in the case of  $V$  groups. Notably, the GPS with  $V = 8$  achieves a performance improvement of approximately 0.4 dB over the enumerated algorithm with  $V = 4$ , while having lower

computational complexity. Consequently, the non-enumerated GPS is deemed more efficient in practical implementations.

## V. CONCLUSION

In this letter, a GPS algorithm is proposed to reduce PAPR in AFDM. We first modify the pre-chirp module of conventional AFDM, ensuring that such an adjustment preserves the inherent characteristics of AFDM. Subsequently, we discuss several factors in GPS to achieve the optimal balance between performance and complexity. Finally, simulations are conducted to verify the performance of GPS. The numerical results show that the adjacent grouping pattern exhibits superior performance compared to the comb grouping pattern. Other better grouping patterns and the allocation of the number of subcarriers per group could be interesting directions for future research.

## REFERENCES

- [1] M. M. Azari, S. Solanki, S. Chatzinotas, O. Kodheli, H. Sallouha, A. Colpaert, J. F. Mendoza Montoya, S. Pollin, A. Haqiqatnejad, A. Mostaani, E. Lagunas, and B. Ottersten, "Evolution of non-terrestrial networks from 5G to 6G: A survey," *IEEE Commun. Surveys Tuts.*, vol. 24, no. 4, pp. 2633–2672, 2022.
- [2] Y. Xu, J. Jiang, D. He, and W. Zhang, "A NB-IoT random access scheme based on change point detection in NTN," *IEEE Open J. Commun. Soc.*, vol. 4, pp. 2176–2185, 2023.
- [3] A. Bemani, N. Ksairi, and M. Kountouris, "AFDM: A full diversity next generation waveform for high mobility communications," in *Proc. IEEE Int. Commun. Conf. Workshops (ICC Workshops)*, Montreal, QC, Canada, 2021, pp. 1–6.
- [4] —, "Affine frequency division multiplexing for next generation wireless communications," *IEEE Trans. Wireless Commun.*, vol. 22, no. 11, pp. 8214–8229, 2023.
- [5] R. Hadani, S. Rakib, M. Tsatsanis, A. Monk, A. J. Goldsmith, A. F. Molisch, and R. Calderbank, "Orthogonal time frequency space modulation," in *Proc. IEEE Wireless Commun. Netw. Conf. (WCNC)*, San Francisco, CA, USA, 2017, pp. 1–6.
- [6] H. S. Rou, G. T. F. de Abreu, J. Choi, M. Kountouris, Y. L. Guan, O. Gonsa *et al.*, "From OTFS to AFDM: A comparative study of next-generation waveforms for ISAC in doubly-dispersive channels," *arXiv preprint arXiv:2401.07700*, 2024.
- [7] H. Yin and Y. Tang, "Pilot aided channel estimation for AFDM in doubly dispersive channels," in *Proc. IEEE/CIC Int. Conf. Commun. China (ICCC)*, Sanshui, Foshan, China, 2022, pp. 308–313.
- [8] A. Bemani, N. Ksairi, and M. Kountouris, "Low complexity equalization for AFDM in doubly dispersive channels," in *Proc. IEEE Int. Conf. Acoust., Speech, Signal Process. (ICASSP)*, Singapore, Singapore, 2022, pp. 5273–5277.
- [9] J. Zhu, Q. Luo, G. Chen, P. Xiao, and L. Xiao, "Design and performance analysis of index modulation empowered AFDM system," *IEEE Wireless Commun. Lett.*, vol. 13, no. 3, pp. 686–690, 2024.
- [10] Q. Luo, P. Xiao, Z. Liu, Z. Wan, N. Thomos, Z. Gao, and Z. He, "AFDM-SCMA: A promising waveform for massive connectivity over high mobility channels," *IEEE Trans. Wireless Commun.*, pp. 1–1, 2024.
- [11] J. Zhu, Y. Tang, F. Liu, X. Zhang, H. Yin, and Y. Zhou, "AFDM-based bistatic integrated sensing and communication in static scatterer environments," *IEEE Wireless Commun. Lett.*, pp. 1–1, 2024.
- [12] R. Roshan, J. Jain, and A. Soni, "Reduction of peak to average power ratio in OFDM technique by using cyclic codes," in *Proc. Int. Conf. Intell. Syst. Signal Process. (ISSP)*, Vallabh Vidyanagar, India, 2013, pp. 233–237.
- [13] S. Gopi and S. Kalyani, "An optimized SLM for PAPR reduction in non-coherent OFDM-IM," *IEEE Wireless Commun. Lett.*, vol. 9, no. 7, pp. 967–971, 2020.
- [14] H. Li, N. Yang, Y. Xu, X. Ou, D. He, and Y. Guan, "On the PAPR of the LTE-based 5G terrestrial broadcast system," in *Proc. IEEE Int. Symp. Broadband Multimedia Syst. Broadcast. (BMSB)*, Beijing, China, 2023, pp. 1–6.
- [15] S. H. Han and J. H. Lee, "An overview of peak-to-average power ratio reduction techniques for multicarrier transmission," *IEEE Wireless Commun.*, vol. 12, no. 2, pp. 56–65, 2005.